RESEARCH ARTICLE

Check for updates

A multi-resonant thermally activated delayed fluorescence emitter with a twisted second-generation carbazole dendron showing suppressed concentration quenching and its use in solution-processed organic light-emitting diodes†

Jingxiang Wang,[a] Yuka Yasuda,[b] Yongxia Ren,[b] Ryo Kondo,[b] David B. Cordes, [iD][a] Hironori Kaji [iD] *[b] and Eli Zysman-Colman [iD] *[a]

Multi-resonant thermally activated delayed fluorescence (MR-TADF) emitters have drawn significant interest for use in organic lighting-emitting diodes (OLEDs) as they typically have bright and narrowband emission. However, their rigid, planar structures result in poor solubility in organic solvents and a tendency to aggregate. This usually results in severe aggregation-caused quenching (ACQ), which hinders in particular, their application in solution-processed OLEDs. Herein, a solution-processable MR-TADF emitter **2,7-tBuCzNB** has been designed, synthesized and studied. The presence of eight *tert*-butyl groups and the use of second-generation donor dendrons help enhance its solubility and suppress the ACQ. **2,7-tBuCzNB** exhibits narrowband green emission at 493 nm, with a full-width at half maximum of 32 nm and a high photoluminescence quantum yield (Φ_{PL}) of 93% in toluene. The Φ_{PL} values in 1–10 wt% doped films in mCP are slightly lower but still reach up to 80%. Solution-processed OLEDs using this emitter showed maximum external quantum efficiencies (EQE$_{max}$) of 11.4 and 10.6% at 5 and 10 wt% doping concentration, respectively. This work demonstrates a strategy to synthesize solution processable MR-TADF emitters for use in solution-processed OLEDs.

Introduction

Organic lighting-emitting diodes (OLEDs) have steadily become a dominant display technology, particularly in mobile devices, smartwatches and televisions, due to their inherent advantages of self-luminescence, wide viewing angle, low energy use and the ability to fabricate flexible and transparent devices.[1–4] Almost all commercial OLEDs are fabricated by vacuum deposition as this technology has been shown to produce high-quality, high-performance devices, partly due to the performance of materials specifically designed and syn-

[a]*Organic Semiconductor Centre, EaStCHEM School of Chemistry, University of St Andrews, St Andrews, Fife, UK, KY16 9ST.*
E-mail: eli.zysman-colman@st-andrews.ac.uk; Fax: +44 (0)1334463808;
Tel: +44 (0) 1334463826
[b]*Institute for Chemical Research, Kyoto University, Uji, Kyoto, 611-0011, Japan.*
E-mail: kaji@scl.kyoto-u.ac.jp; Tel: +81 -0774-38-3149

thesized to be compatible with vacuum thermal evaporation. Compared to this fabrication process, solution-processed OLEDs (SP-OLEDs), especially those based on ink-jet printing technology, have distinct advantages, namely a much lower production cost, a more facile fabrication process for large-area devices, and a lower level of material waste.[5,6] Historically, however, SP-OLEDs have tended to show poorer performance than vacuum-deposited OLEDs (VD-OLEDs) in terms of their luminescence efficiency, device lifetime, and color purity. This is in part due to sub-optimal material performance and design.[7–10] Developing new materials specifically targeted for SP-OLEDs remains an outstanding academic and industry research challenge.

Over the past decade, thermally activated delayed fluorescence (TADF) emitters have been widely explored as emitters in OLEDs, partly owing to their ability to harness all of the singlet and triplet excitons to produce light and thus achieve up to 100% internal quantum efficiency (IQE).[11–14] A weak overlap between the highest occupied molecular orbital (HOMO) and the lowest unoccupied molecular orbital (LUMO) is required to achieve a small singlet–triplet energy gap (ΔE_{ST}) that is necessary to promote the required endothermic reverse

intersystem crossing (RISC) underpinning the TADF mechanism.[15] This is typically achieved by the emitter adopting a strongly twisted donor–acceptor (D–A) architecture. However, the long-range charge transfer (LRCT) character of the emissive excited state and the corresponding relatively large structural relaxation upon exciton formation lead to an undesired broadening of the emission envelope, which results in devices having poor color saturation.[16]

In 2016, Hatakeyama *et al.* reported a new type of organic TADF material known as multi-resonant TADF (MR-TADF) emitters.[17,18] The short-range charge transfer (SRCT) character of the emissive lowest singlet (S_1) state that exists as a result of the HOMO/LUMO separation on adjacent atoms and the rigid structure of the molecule result in narrowband emission, small Stokes shifts, and high photoluminescence quantum yields (Φ_{PL}), all of which contribute to devices having high color purity and high maximum external quantum efficiencies (EQE$_{max}$).[19] However, the commonly rigid and planar geometries of MR-TADF emitters lead to poor solubility in organic solvents, causing them to aggregate.[20,21] The resultant poor film-forming properties from solution and severe aggregation-caused quenching (ACQ) are detrimental to their performance in SP-OLEDs.[8,22]

In this report, a new MR-TADF emitter **2,7-tBuCzNB** has been developed to address these outstanding issues in the context of SP-OLEDs (Fig. 1). The asymmetric B–N core (named **Cz-SCz**), reported recently by Ni *et al.*, has been confirmed to have an emissive SRCT state in both toluene and doped films in mCP.[23] The eight *tert*-butyl groups in **2,7-tBuCzNB** are responsible for its good solubility in organic solvents. This property coupled with the relatively high molecular weight of **2,7-tBuCzNB** (1525 g mol^{-1}) contributes to the good film-forming ability of this compound.[24,25] The peripheral *tert*-butyl carbazole and twisted second-generation *tert*-butyl carbazole donors help increase the intermolecular distance between adjacent emitter molecules and suppress ACQ. As a result, **2,7-tBuCzNB** emits at an emission peak wavelength (λ_{PL}) of 500 nm (full width at half maximum, FWHM, of 44 nm) in a 5 wt% doped film in mCP. It has a high Φ_{PL} of 93% in toluene, and the Φ_{PL} values in doped films are around 80% at concentrations ranging from 1 to 10 wt%. The SP-OLEDs using this emitter at a doping concentration of 5 wt% in the DMIC-TRZ

host showed an EQE$_{max}$ of 11.6%, with a low turn on voltage (V_{on}) of 3.4 V. The device with 10 wt% emitter showed nearly the same performance as that with 5 wt% emitter.

Results and discussion

Synthesis

The synthesis of **2,7-tBuCzNB** is shown in Fig. 2. The nitrogen atom of 2,7-dibromo-9H-carbazole was firstly protected using *tert*-butyldimethylsilyl chloride to obtain **1** in 93% yield. Compound **1** was reacted with 3,6-di-*tert*-butyl-9H-carbazole under Buchwald–Hartwig cross-coupling conditions to afford **2** in 81% yield, which was subsequently deprotected to afford **3** in 91% yield. Compound **3** was employed in a twofold S$_N$Ar reaction with 2,6-difluorobromobenzene to afford **4** in 35% yield. **2,7-tBuCzNB** was obtained *via* a lithium–halogen exchange/intramolecular borylation cyclization cascade in 12% yield. The identity and purity of this compound were characterized using melting point determination, ^{1}H and ^{13}C nuclear magnetic resonance (NMR) spectroscopy, high-resolution mass spectrometry (HRMS), high-performance liquid chromatography (HPLC), and elemental analysis (EA) (Fig. S1–S17†). The structure of **2,7-tBuCzNB** was confirmed by single crystal X-ray diffraction analysis (Fig. 3a, Fig. S18, and Table S2†).

Theoretical calculations

The optimized ground-state geometry and energy levels of **2,7-tBuCzNB** were calculated using Density Functional Theory (DFT) at the PBE0/6-31G(d,p) level (Fig. 3b), starting from a structure drawn and optimized using Chem3D.[26,27] The LUMO is localized on the **Cz-SCz** core. The calculated LUMO level of −1.87 eV is slightly more stabilized than that of **Cz-SCz** (−1.68 eV) (Fig. S19†). The HOMO is distributed on the peripheral twisted second-generation carbazole donor dendron due to its strong electron-donating character. The calculated HOMO energy of **2,7-tBuCzNB** is −5.18 eV, which is close to that of **2GCzBP** (HOMO of −5.19 eV)[28] and **2GCzBPN** (HOMO of −5.25 eV),[29] both containing a regioisomeric second-generation carbazole donor dendron. The different regiochemistry of the peripheral *tert*-carbazole groups does not have a significant effect on the energy level. The excited-state energies were first
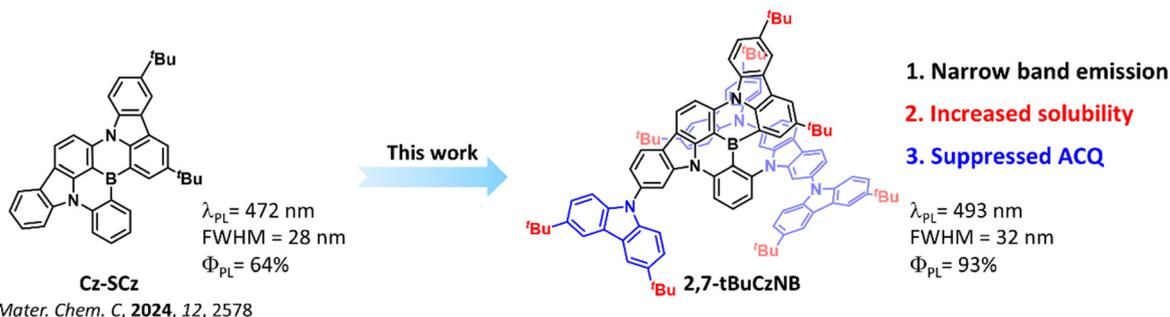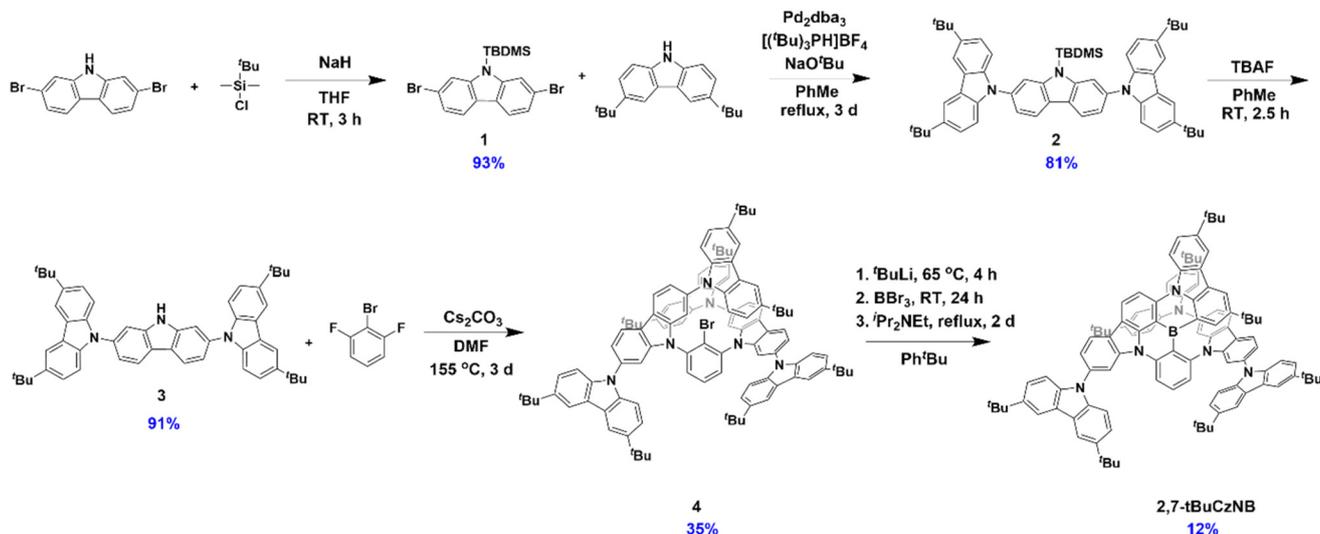

Fig. 1 Molecular design of **2,7-tBuCzNB**.

3280 | *Org. Chem. Front.*, 2025, **12**, 3279–3287

This journal is © the Partner Organisations 2025

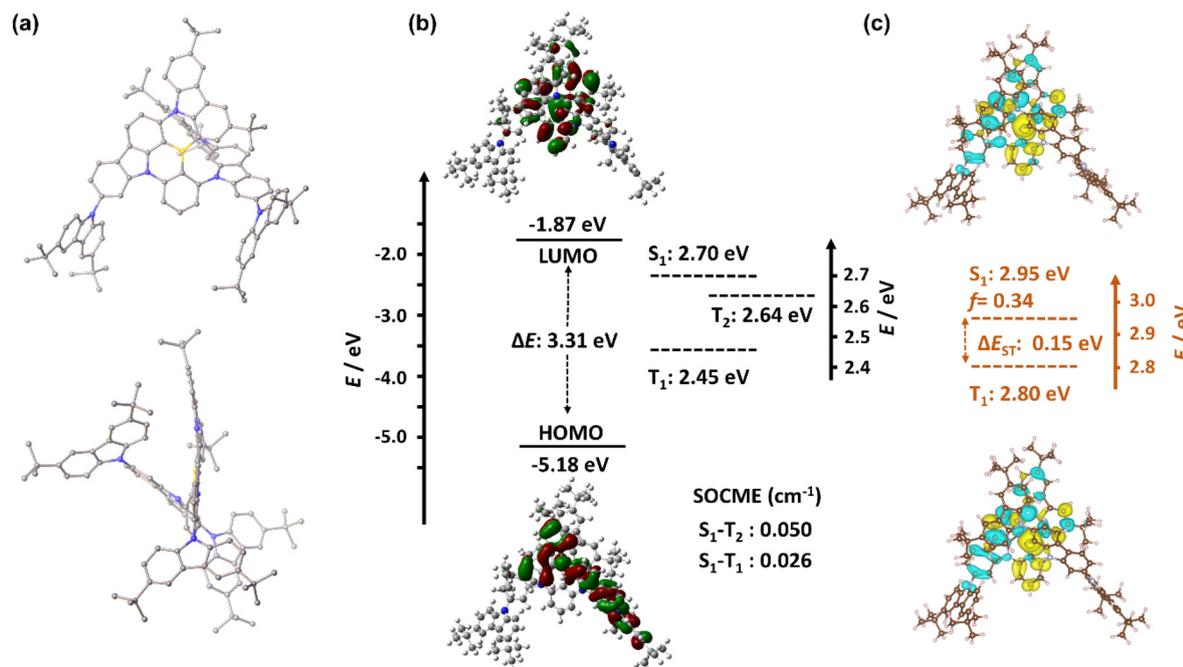**Fig. 2** Synthesis scheme of **2,7-tBuCzNB**.

Fig. 3 (a) Two views of one molecule in the structure of **2,7-tBuCzNB**. Minor components of disorder and hydrogen atoms have been omitted for clarity. (b) Calculated HOMO, LUMO and energy level diagram based on the optimized ground-state geometry and SOCME values based on the optimized T_1 geometry in the gas phase at PBE0/6-31G(d,p). (c) Difference density plots of S_1 and T_1 for **2,7-tBuCzNB** calculated in the gas phase at the SCS-ADC2/cc-pVDZ level (blue indicates an area of decreased electron density while yellow indicates increased electronic density between the ground and excited states).

calculated using time-dependent DFT within the Tamm–Dancoff approximation (TDA-DFT) at the PBE0/6-31G(d,p) level (Fig. 3b). The S_1 state and the lowest triplet state (T_1) energies are 2.70/2.45 eV and the corresponding ΔE_{ST} value is 0.25 eV. Spin–orbit coupling matrix elements (SOCME) were calculated based on the optimized T_1 geometry at the PBE0/6-31G(d,p) level, with **2,7-tBuCzNB** showing similar SOCME values of 0.026 and

0.050 cm^{-1} for the S_1–T_1 and S_1–T_2 transitions, respectively. The larger SOCME and smaller energy gaps between S_1 and T_2 indicate that RISC may proceed *via* T_2 to S_1.[30–34]

Spin-component scaling second-order algebraic diagrammatic construction (SCS-(ADC)2/cc-pVDZ) calculations provide more accurate predictions of the excited-state energies and difference densities in MR-TADF compounds compared to

TD-DFT methods (Fig. 3c).[21,35,36] The alternating difference density patterns for both the S_1 and T_1 states are localized on the **Cz-SCz** core, indicating that these states have SRCT character. The S_1/T_1 energies are calculated to be 2.95/2.80 eV and the corresponding ΔE_{ST} value is 0.15 eV. Both the difference densities and the small ΔE_{ST} indicate the likelihood of **2,7-tBuCzNB** being a MR-TADF emitter.

Optoelectronic properties

The HOMO and LUMO values of **2,7-tBuCzNB** were extrapolated from the electrochemical measurements in degassed acetonitrile containing 0.1 M [$^nBu_4N$]PF_6 as the supporting electrolyte and Fc/Fc$^+$ as the internal reference (0.38 V vs. SCE)[37] (Fig. S20†). The electrochemical data are summarized in Table S3.† The cyclic voltammogram of **2,7-tBuCzNB** shows reversible oxidation and reduction waves with an oxidation potential (E_{ox}) of 1.04 V vs. SCE, and a reduction potential (E_{red}) of −1.71 V vs. SCE, values that were obtained from the peaks of the corresponding differential pulse voltammogram. The corresponding HOMO and LUMO energies are −5.46 and −2.71 eV, and the ΔE value is calculated to be 2.75 eV. The HOMO energy is similar to those of most emitters containing regioisomeric second-generation carbazole donor dendrons (HOMOs of −5.41 and −5.40 eV for **tBuCz3pTRZ** and **tBuCz3mTRZ**[38] and −5.41 eV for **tBuCz2pTRZ**, **tBuCz2mTRZ**, and **tBuCz2m2pTRZ**[39]), and the LUMO energy is nearly the same as that of **Cz-SCz** (LUMO of −2.74 eV),[23] indicating that oxidation occurs on the central carbazole of the second-generation carbazole donor, while reduction occurs on the B–N core.

The ultraviolet-visible (UV-vis) absorption and photoluminescence (PL) spectra of **2,7-tBuCzNB** in dilute toluene are shown in Fig. 4a. The low-energy absorption band at a peak wavelength (λ_{abs}) of 465 nm (molar absorptivity, ε, of 4.8×10^4 M^{-1} cm^{-1}), similar to those of both **Cz-SCz** (λ_{abs} of 451 nm)[23] and **DtBuCzB** (λ_{abs} of 467 nm),[40] can be attributed to the SRCT S_0–S_1 absorption transitions. **2,7-tBuCzNB** emits at λ_{PL} of

493 nm with a relatively narrow FWHM of 32 nm/0.16 eV. The bathochromic shifting of the absorption and emission spectra compared to **Cz-SCz** (λ_{PL} of 472 nm)[23] indicates that the additional carbazole and second-generation carbazole donors affect the electronic properties of the **Cz-SCz** core. The slightly broader emission compared to that of **Cz-SCz** (FWHM of 28 nm)[23] can be attributed to the larger degree of geometry relaxation because of the additional donors. The Φ_{PL} value of **2,7-tBuCzNB** in degassed toluene is 93%. There is a very small degree of positive solvatochromism, which indicates that the SRCT character of the S_1 state is conserved across this family of solvents (Fig. 4b).

The steady-state PL and phosphorescence spectra of **2,7-tBuCzNB** in 2-methyltetrahydrofuran (2-MeTHF) at 77 K were measured to determine the ΔE_{ST} (Fig. 5a). The singlet and triplet energies, determined from the difference in the onset energies of the steady-state PL and phosphorescence spectra, are 2.59 and 2.43 eV, respectively, resulting in a ΔE_{ST} of 0.16 eV, a value that is similar to the calculated value (ΔE_{ST} of 0.15 eV) and that of **Cz-SCz** (ΔE_{ST} of 0.18 eV).[23] Time-resolved PL studies in toluene revealed monoexponential decay kinetics, with a fast prompt lifetime (τ_p) of 6.6 ns (Fig. 5b). No delayed emission was observed in toluene solution, which is due to the magnitude of the ΔE_{ST} and the competing non-radiative decay processes to ISC/RISC cycling.[41]

The photophysical properties of thin films were then investigated. 1,3-Bis(N-carbazolyl) benzene (mCP) was first used as the host material because of its suitably high triplet energy (E_T = 2.9 eV).[42] The absolute Φ_{PL} values of **2,7-tBuCzNB** at different doping concentrations in mCP were measured under a nitrogen atmosphere (Table S4†). The 1, 5 and 10 wt% doped films of **2,7-tBuCzNB** in mCP have similar yet slightly red-shifted PL spectra, peaking at λ_{PL} of 496, 500 and 504 nm (FWHM of 41, 44 and 48 nm), while the corresponding Φ_{PL} values remain high at 80, 81 and 77% (Fig. S21†). Although the Φ_{PL} values are slightly lower than those in toluene, the concentration quenching is negligible in this concentration
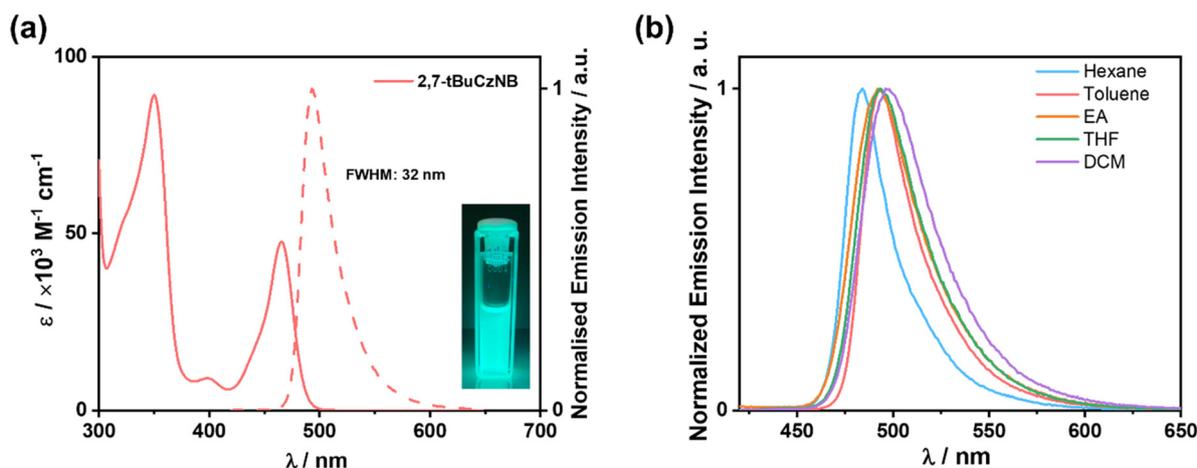

Fig. 4 (a) UV-vis absorption and PL spectra of **2,7-tBuCzNB** in toluene at 300 K. Inset: photo of **2,7-tBuCzNB** in toluene excited at 365 nm. (b) PL spectra of **2,7-tBuCzNB** in different solvents at 300 K. (λ_{exc} = 340 nm).

3282 | *Org. Chem. Front.*, 2025, **12**, 3279–3287
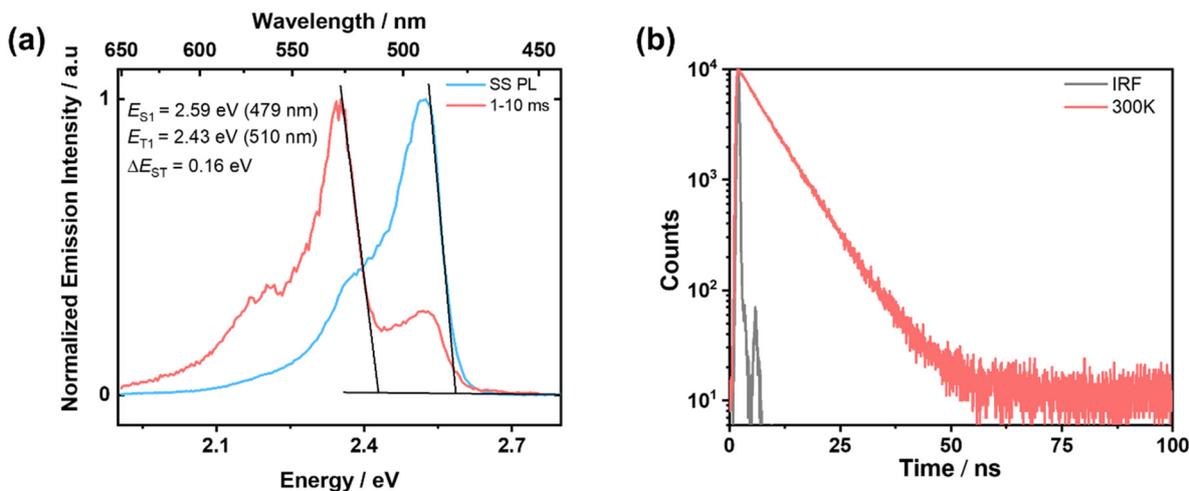
This journal is © the Partner Organisations 2025

Fig. 5 (a) Steady-state PL and phosphorescence spectra of **2,7-tBuCzNB** (λ_{exc} = 340 nm). (b) Time-resolved PL decay of **2,7-tBuCzNB** in degassed toluene (λ_{exc} = 375 nm).

range. When increasing the doping concentrations to 20 and 50 wt%, the PL spectra broaden and further red-shift to λ_{PL} of 509 and 516 nm (FWHM of 52 and 65 nm), respectively, as aggregation of the emitters becomes pronounced; the Φ_{PL} values decrease precipitously to 61 and 36%, respectively (Fig. S21†).

Having identified that the 5 wt% doped film in mCP is optimal, we next proceeded to obtain the steady-state PL spectra and time-resolved PL decays. This film emits at λ_{PL} of 500 nm and has a FWHM of 44 nm/0.21 eV (Fig. 6a). In contrast to the properties of the isolated molecules in dilute solution, the intermolecular interactions between host–guest and guest–guest cannot be avoided in the film state, which leads to a weak red-shift and broadening of the PL spectrum of the 5 wt% doped films compared to those in toluene (λ_{PL} of 493 nm, FWHM of 32 nm/0.16 eV). The ΔE_{ST} value is slightly smaller at 0.13 eV compared to that in 2-MeTHF (Fig. 6b). The

time-resolved PL decay at 300 K under vacuum reveals a prompt fluorescence lifetime, τ_p, of 7.6 ns and a long delayed lifetime, τ_d, of 1.2 ms (Table 1). The increase in the intensity of delayed emission with the increase in temperature from 77 to 300 K confirms the presence of TADF (Fig. 6c). The much longer τ_d of **2,7-tBuCzNB** compared to that of **Cz-SCz** (τ_d of 425 μs)[23] may be due to the much lower SOCME values (0.026 and 0.050 cm^{-1} for S_1–T_1 and S_1–T_2 of **2,7-tBuCzNB** compared to 0.150 and 0.653 cm^{-1} for S_1–T_1 and S_1–T_2 of **Cz-SCz**) (Fig. S19†), which result in a lower RISC rate constant (k_{RISC} = 5.4 × 10^2 s^{-1}, Table S5†). The time-resolved PL decay of the 10 wt% doped film in mCP was also measured (Fig. S22†). The similar PL spectra, Φ_{PL} values, and prompt and delayed lifetimes of the 10 wt% doped film and the 5 wt% doped film indicate that there is a negligible impact of changing the concentration of the emitter on the photophysical properties (Table 1).
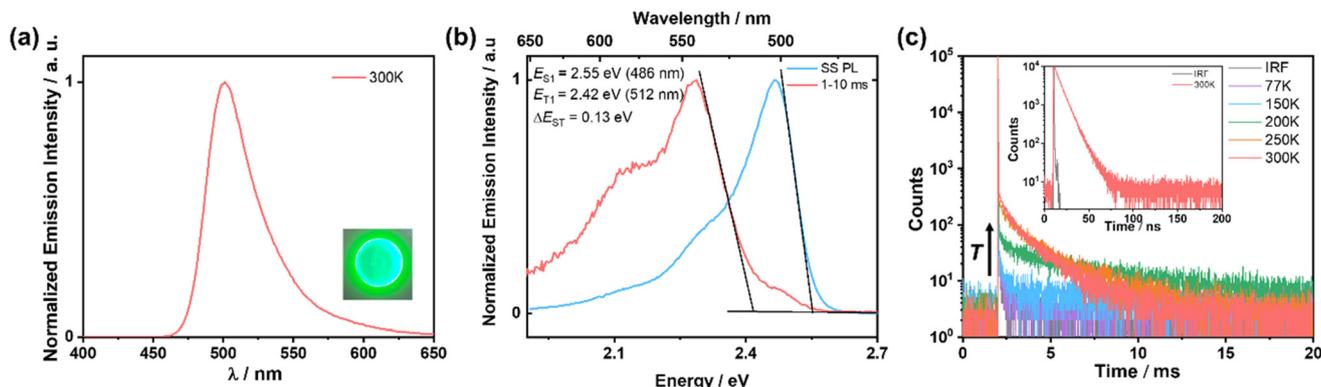

Fig. 6 (a) Steady-state PL spectra in the 5 wt% doped film in mCP (λ_{exc} = 340 nm). Inset: photo of the doped film excited at 365 nm. (b) Steady-state PL and phosphorescence spectra of the 5 wt% doped film of **2,7-tBuCzNB** in mCP measured in the film at 77 K (λ_{exc} = 340 nm). (c) Variable temperature time-resolved PL decays of the 5 wt% doped film of **2,7-tBuCzNB** in mCP (λ_{exc} = 375 nm).

This journal is © the Partner Organisations 2025

Org. Chem. Front., 2025, **12**, 3279–3287 | **3283**

Table 1 Photophysical data of **2,7-tBuCzNB**

In PhMe	λ_{abs}/nm	λ_{PL} (FWHM)/nm	Φ_{PL}/%	ΔE_{ST}/eV	In film	λ_{PL} (FWHM)/nm	Φ_{PL}/%	τ_p/ns	τ_d/ms
	465	493 (32)	93	0.16	5 wt%	500 (44)	81	7.6	1.2
					10 wt%	504 (48)	77	6.8	1.2

Organic light-emitting diodes

Finally, we fabricated SP-OLEDs with **2,7-tBuCzNB** as the emitter. We report herein the device data using 5-(3-(4,6-diphenyl-1,3,5-triazin-2-yl)phenyl)-7,7-dimethyl-5,7-dihydroindeno[2,1-*b*]carbazole (DMIC-TRZ) as the host, as it afforded higher efficiency devices (see the ESI for results of SP-OLEDs using mCP:30 wt% OXD-7 as a mixed host, Fig. S23, and Table S6†). The device structure consisted of indium tin oxide (ITO) (50 nm)/poly(styrenesulfonic acid)-doped poly(3,4-ethylenedioxythiophene) (PEDOT:PSS) (45 nm)/poly(*N*-vinylcarbazole) (PVK) (15 nm)/*X* wt% **2,7-tBuCzNB**:DMIC-TRZ (30 nm)/2,4,6-tris[3-(diphenylphosphinyl)phenyl]-1,3,5-triazine (PO-T2T) (20 nm)/4,6-bis(3,5-di-4-pyridinylphenyl)-2-methylpyrimidine (B4PyMPM) (35 nm)/lithium fluoride (LiF) (1 nm)/Al (100 nm). Here, we employed PEDOT:PSS for hole injection, PVK for hole transport and electron blocking, PO-T2T for electron transport and hole and exciton blocking, B4PyMPM for electron transport, and LiF for electron injection. ACQ is suppressed in **2,7-tBuCzNB**, allowing the fabrication of devices at relatively higher doping concentrations than those typically used for MR-TADF OLEDs; here, doping concentrations of 5 and 10 wt% are used. The device structure and performance are shown in Fig. 7 and Table 2. The 5 wt% doped SP-OLEDs
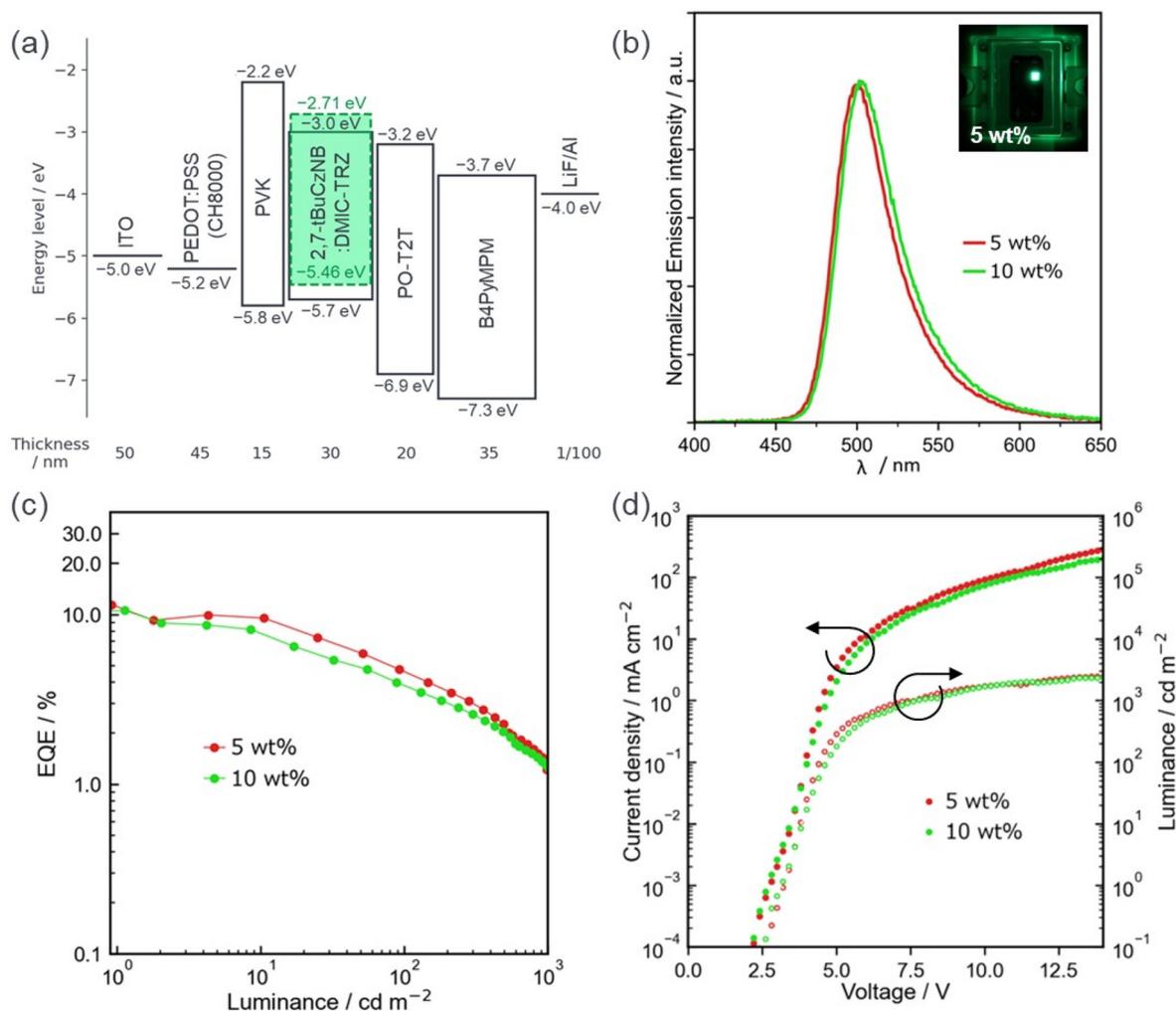

Fig. 7 (a) Device structure, (b) electroluminescence spectra (inset: photograph of the 5 wt% device), (c) EQE–luminance curves, and (d) current density–voltage–luminance characteristics of SP-OLEDs using 5 or 10 wt% **2,7-tBuCzNB**:DMIC-TRZ as the emitting layer.

Table 2 Φ_{PL} and device performances of **2,7-tBuCzNB** in DMIC-TRZ

Doped concentration	$\Phi_{PL}{}^{a}$/%	$EQE_{max}/EQE_{100}{}^{b}$/%	$V_{on}{}^{c}$/V	λ_{EL} (FWHM)^{d}/nm	CIE^{e} (x, y)
5 wt%	94	11.4/4.6	3.4	500 (41)	(0.16, 0.56)
10 wt%	90	10.6/3.8	3.2	503 (42)	(0.17, 0.59)

^{a} Measured in the doped film in DMIC-TRZ. ^{b} Maximum EQE and EQE at 100 cd m^{-2}. ^{c} Turn-on voltage at 1 cd m^{-2}. ^{d} EL peak wavelength and FWHM. ^{e} CIE coordinates at 1 mA cm^{-2} for the **2,7-tBuCzNB**:DMIC-TRZ devices.

exhibited pure green emission at λ_{EL} of 500 nm (FWHM of 41 nm) and associated CIE coordinates of (0.16, 0.56), which is effectively identical to the PL spectra. The EQE_{max} for this device was 11.4%. The 10 wt% doped device showed almost the same results, but with a slightly lower EQE_{max} of 10.6%, confirming the suppression of ACQ of the emission of **2,7-tBuCzNB**. Unfortunately, despite the high Φ_{PL} values, these devices exhibited significant efficiency roll-off, with relatively low EQE values at high luminance (EQE values of 4.6 and 3.8% at 100 cd m^{-2} for 5 and 10 wt% doped devices, respectively), probably associated with the extremely slow RISC.

Conclusion

A new solution-processable MR-TADF emitter, **2,7-tBuCzNB**, has been designed and synthesized. The SCS-(ADC)2 calculations, the narrowband emission at 493 nm (FWHM of 32 nm) in toluene and the weakly positive solvatochromism all corroborate that the emissive S_1 state possesses SRCT character. The introduction of twisted second-generation *tert*-butyl carbazole donor dendrons alleviates ACQ in films at doping concentrations of 10 wt%. Solution-processed OLEDs with **2,7-tBuCzNB** as the emitter fabricated at 5 or 10 wt% doping concentration exhibited similar performance in terms of their narrowband EL spectra peaking at around 500 nm (FWHM around 40 nm), EQE_{max} of 11% and low V_{on} around 3 V.

Data availability

The research data supporting this publication can be accessed at https://doi.org/10.17630/76dc4617-0c93-45f6-9c8c-340e5112c325.

Conflicts of interest

The authors declare no conflict of interest.

Acknowledgements

References

1 C. W. Tang and S. A. VanSlyke, Organic electroluminescent diodes, *Appl. Phys. Lett.*, 1987, **51**, 913–915.

2 R. H. Friend, R. Gymer, A. Holmes, J. Burroughes, R. Marks, C. Taliani, D. Bradley, D. D. Santos, J.-L. Bredas and M. Lögdlund, Electroluminescence in conjugated polymers, *Nature*, 1999, **397**, 121–128.

3 J. Park, D. Shin and S. Park, Large-area OLED lightings and their applications, *Semicond. Sci. Technol.*, 2011, **26**, 034002.

4 S. R. Forrest, The path to ubiquitous and low-cost organic electronic appliances on plastic, *Nature*, 2004, **428**, 911–918.

5 T. Huang, W. Jiang and L. Duan, Recent progress in solution processable TADF materials for organic light-emitting diodes, *J. Mater. Chem. C*, 2018, **6**, 5577–5596.

6 J. Y. Woo, M. H. Park, S. H. Jeong, Y. H. Kim, B. Kim, T. W. Lee and T. H. Han, Advances in Solution-Processed OLEDs and their Prospects for Use in Displays, *Adv. Mater.*, 2023, **35**, 2207454.

7 N. Ikeda, S. Oda, R. Matsumoto, M. Yoshioka, D. Fukushima, K. Yoshiura, N. Yasuda and T. Hatakeyama, Solution-Processable Pure Green Thermally Activated Delayed Fluorescence Emitter Based on the Multiple Resonance Effect, *Adv. Mater.*, 2020, **32**, 2004072.

8 X. Cai, Y. Xu, Y. Pan, L. Li, Y. Pu, X. Zhuang, C. Li and Y. Wang, Solution–Processable Pure–Red Multiple Resonance–induced Thermally Activated Delayed Fluorescence Emitter for Organic Light–Emitting Diode with External Quantum Efficiency over 20%, *Angew. Chem., Int. Ed.*, 2023, **62**, e202216473.

9 Y. Zou, S. Gong, G. Xie and C. Yang, Design Strategy for Solution–Processable Thermally Activated Delayed

This journal is © the Partner Organisations 2025

Org. Chem. Front., 2025, **12**, 3279–3287 | **3285**

Fluorescence Emitters and Their Applications in Organic Light–Emitting Diodes, *Adv. Opt. Mater.*, 2018, **6**, 1800568.

10 D. Liu, W. Tian, Y. Feng, X. Zhang, X. Ban, W. Jiang and Y. Sun, Achieving 20% External Quantum Efficiency for Fully Solution-Processed Organic Light-Emitting Diodes Based on Thermally Activated Delayed Fluorescence Dendrimers with Flexible Chains, *ACS Appl. Mater. Interfaces*, 2019, **11**, 16737–16748.

11 H. Uoyama, K. Goushi, K. Shizu, H. Nomura and C. Adachi, Highly Efficient Organic Light-Emitting Diodes from Delayed Fluorescence, *Nature*, 2012, **492**, 234–238.

12 M. Y. Wong and E. Zysman-Colman, Purely Organic Thermally Activated Delayed Fluorescence Materials for Organic Light–Emitting Diodes, *Adv. Mater.*, 2017, **29**, 1605444.

13 J. Marques dos Santos, D. Hall, B. Basumatary, M. Bryden, D. Chen, P. Choudhary, T. Comerford, E. Crovini, A. Danos, J. De, S. Diesing, M. Fatahi, M. Griffin, A. K. Gupta, H. Hafeez, D. Karthik, L. Hämmerling, E. Hanover, J. Haug, T. Heil, S. Kumar, O. Lee, H. Li, F. Lucas, C. F. R. Mackenzie, A. Mariko, T. Matulaitis, F. Millward, Y. Olivier, S. Pagidi, Q. Qi, I. D. W. Samuel, N. Sharma, C. Si, L. Spierling, D. Sun, E. Tankelevičiūtė, M. D. Tonet, J. Wang, T. Wang, S. Wu, Y. Xu, L. Zhang and E. Zysman-Colman, The Golden Age of Thermally Activated Delayed Fluorescence Materials: Design and Exploitation, *Chem. Rev.*, 2024, **124**(24), 13736–14110.

14 H. Kaji, H. Suzuki, T. Fukushima, K. Shizu, K. Suzuki, S. Kubo, T. Komino, H. Oiwa, F. Suzuki, A. Wakamiya, Y. Murata and C. Adachi, Purely organic electroluminescent material realizing 100% conversion from electricity to light, *Nat. Commun.*, 2015, **6**, 8476.

15 Q. Zhang, J. Li, K. Shizu, S. Huang, S. Hirata, H. Miyazaki and C. Adachi, Design of Efficient Thermally Activated Delayed Fluorescence Materials for Pure Blue Organic Light Emitting Diodes, *J. Am. Chem. Soc.*, 2012, **134**, 14706–14709.

16 Y. Im, M. Kim, Y. J. Cho, J.-A. Seo, K. S. Yook and J. Y. Lee, Molecular Design Strategy of Organic Thermally Activated Delayed Fluorescence Emitters, *Chem. Mater.*, 2017, **29**, 1946–1963.

17 T. Hatakeyama, K. Shiren, K. Nakajima, S. Nomura, S. Nakatsuka, K. Kinoshita, J. Ni, Y. Ono and T. Ikuta, Ultrapure blue thermally activated delayed fluorescence molecules: efficient HOMO–LUMO separation by the multiple resonance effect, *Adv. Mater.*, 2016, **28**, 2777–2871.

18 H. Hirai, K. Nakajima, S. Nakatsuka, K. Shiren, J. Ni, S. Nomura, T. Ikuta and T. Hatakeyama, One-Step Borylation of 1,3-Diaryloxybenzenes Towards Efficient Materials for Organic Light-Emitting Diodes, *Angew. Chem., Int. Ed.*, 2015, **54**, 13581–13585.

19 H. J. Kim and T. Yasuda, Narrowband Emissive Thermally Activated Delayed Fluorescence Materials, *Adv. Opt. Mater.*, 2022, **10**, 2201714.

20 S. Xu, Q. Yang, Y. Zhang, H. Li, Q. Xue, G. Xie, M. Gu, J. Jin, L. Huang and R. Chen, Solution-processed multi-resonance organic light-emitting diodes with high

efficiency and narrowband emission, *Chin. Chem. Lett.*, 2021, **32**, 1372–1376.

21 J. Wang, H. Hafeez, S. Tang, T. Matulaitis, L. Edman, I. D. Samuel and E. Zysman-Colman, Highly efficient organic light–emitting diodes and light–emitting electrochemical cells employing multiresonant thermally activated delayed fluorescent emitters with bulky donor or acceptor peripheral groups, *Aggregate*, 2024, e571.

22 B. Du, K. Zhang, P. Wang, X. Wang, S. Wang, S. Shao and L. Wang, Spirofluorene-Locked Carbazole Based Multiple Resonance Thermally Activated Delayed Fluorescence Emitters for Efficient Solution-Processed Narrowband Green OLEDs, *J. Mater. Chem. C*, 2023, **11**, 9578–9585.

23 H.-X. Ni, X.-F. Luo, L. Yuan, J.-J. Hu, W.-W. Zhang and Y.-X. Zheng, Asymmetric multiple resonance thermally activated delayed fluorescence emitters for sky-blue and pure blue electroluminescence, *J. Mater. Chem. C*, 2024, **12**, 2578–2584.

24 T. Wang, X. Yin, X. Cao and C. Yang, A Simple Approach to Solution–Processible Small–Molecule Multi–Resonance TADF Emitters for High–Performance Narrowband OLEDs, *Angew. Chem., Int. Ed.*, 2023, **62**, e202301988.

25 J. Hwang, H. Kang, J.-E. Jeong, H. Y. Woo, M. J. Cho, S. Park and D. H. Choi, Donor engineered Deep-Blue emitters for tuning luminescence mechanism in Solution-Processed OLEDs, *Chem. Eng. J.*, 2021, **416**, 129185.

26 T. H. Dunning, Jr., Gaussian basis sets for use in correlated molecular calculations. I. The atoms boron through neon and hydrogen, *J. Chem. Phys.*, 1989, **90**, 1007–1023.

27 C. Adamo and V. Barone, Toward reliable density functional methods without adjustable parameters: The PBE0 model, *J. Chem. Phys.*, 1999, **110**, 6158–6170.

28 C. Si, D. Sun, T. Matulaitis, D. B. Cordes, A. M. Z. Slawin and E. Zysman-Colman, Rational molecular design of efficient yellow-red dendrimer TADF for solution-processed OLEDs: a combined effect of substitution position and strength of the donors, *Sci. China: Chem.*, 2024, **67**, 1613–1623.

29 C. Si, T. Wang, Y. Xu, D. Lin, D. Sun and E. Zysman-Colman, A temperature sensor with a wide spectral range based on a dual-emissive TADF dendrimer system, *Nat. Commun.*, 2024, **15**, 7439.

30 X. Cao, K. Pan, J. Miao, X. Lv, Z. Huang, F. Ni, X. Yin, Y. Wei and C. Yang, Manipulating Exciton Dynamics toward Simultaneous High-Efficiency Narrowband Electroluminescence and Photon Upconversion by a Selenium-Incorporated Multiresonance Delayed Fluorescence Emitter, *J. Am. Chem. Soc.*, 2022, **144**, 22976–22984.

31 I. S. Park, H. Min and T. Yasuda, Ultrafast Triplet-Singlet Exciton Interconversion in Narrowband Blue Organoboron Emitters Doped with Heavy Chalcogens, *Angew. Chem., Int. Ed.*, 2022, **61**, e202205684.

32 I. Kim, K. H. Cho, S. O. Jeon, W. J. Son, D. Kim, Y. M. Rhee, I. Jang, H. Choi and D. S. Kim, Three States Involving Vibronic Resonance is a Key to Enhancing Reverse Intersystem Crossing Dynamics of an Organoboron-Based Ultrapure Blue Emitter, *JACS Au*, 2021, **1**, 987–997.

3286 | *Org. Chem. Front.*, 2025, **12**, 3279–3287

This journal is © the Partner Organisations 2025

33 K. Shizu and H. Kaji, Quantitative prediction of rate constants and its application to organic emitters, *Nat. Commun.*, 2024, **15**, 4723.

34 K. Shizu and H. Kaji, Comprehensive understanding of multiple resonance thermally activated delayed fluorescence through quantum chemistry calculations, *Commun. Chem.*, 2022, **5**, 53.

35 A. Pershin, D. Hall, V. Lemaur, J. C. Sancho-Garcia, L. Muccioli, E. Zysman-Colman, D. Beljonne and Y. Olivier, Highly emissive excitons with reduced exchange energy in thermally activated delayed fluorescent molecules, *Nat. Commun.*, 2019, **10**, 597.

36 D. Hall, J. C. Sancho-García, A. Pershin, G. Ricci, D. Beljonne, E. Zysman-Colman and Y. Olivier, Modeling of Multiresonant Thermally Activated Delayed Fluorescence Emitters - Properly Accounting for Electron Correlation Is Key!, *J. Chem. Theory Comput.*, 2022, **18**, 4903–4918.

37 V. V. Pavlishchuk and A. W. Addison, Conversion constants for redox potentials measured versus different reference electrodes in acetonitrile solutions at 25 C, *Inorg. Chim. Acta*, 2000, **298**, 97–102.

38 D. Sun, R. Saxena, X. Fan, S. Athanasopoulos, E. Duda, M. Zhang, S. Bagnich, X. Zhang, E. Zysman-Colman and A. Köhler, Regiochemistry of Donor Dendrons Controls the Performance of Thermally Activated Delayed Fluorescence Dendrimer Emitters for High Efficiency Solution-Processed Organic Light-Emitting Diodes, *Adv. Sci.*, 2022, **9**, 2201470.

39 D. Sun, E. Duda, X. Fan, R. Saxena, M. Zhang, S. Bagnich, X. Zhang, A. Köhler and E. Zysman-Colman, Thermally Activated Delayed Fluorescent Dendrimers that Underpin High-Efficiency Host-Free Solution-Processed Organic Light-Emitting Diodes, *Adv. Mater.*, 2022, **34**, 2110344.

40 Y. Xu, Z. Cheng, Z. Li, B. Liang, J. Wang, J. Wei, Z. Zhang and Y. Wang, Molecular–Structure and Device–Configuration Optimizations toward Highly Efficient Green Electroluminescence with Narrowband Emission and High Color Purity, *Adv. Opt. Mater.*, 2020, **8**, 1902142.

41 X. Wu, B.-K. Su, D.-G. Chen, D. Liu, C.-C. Wu, Z.-X. Huang, T.-C. Lin, C.-H. Wu, M. Zhu, E. Y. Li, W.-Y. Hung, W. Zhu and P.-T. Chou, The role of host–guest interactions in organic emitters employing MR-TADF, *Nat. Photonics*, 2021, **15**, 780–786.

42 M. H. Tsai, Y. H. Hong, C. H. Chang, H. C. Su, C. C. Wu, A. Matoliukstyte, J. Simokaitiene, S. Grigalevicius, J. V. Grazulevicius and C. P. Hsu, 3−(9−Carbazolyl) carbazoles and 3, 6−Di (9−carbazolyl) carbazoles as effective host materials for efficient blue organic electrophosphorescence, *Adv. Mater.*, 2007, **19**, 862–866.

This journal is © the Partner Organisations 2025

Org. Chem. Front., 2025, **12**, 3279–3287 | **3287**